CAPACITY-DEMAND DIAGRAM METHODS BASED ON INELASTIC DESIGN SPECTRUM

Anil K CHOPRA[1] And Rakesh K GOEL[2]

SUMMARY

An improved capacity-demand-diagram method that uses the well-known constant-ductility design spectrum for the demand diagram is developed and illustrated by examples. This method estimates the deformation of inelastic SDF systems consistent with the selected inelastic design spectrum, while retaining the attraction of graphical implementation of the ATC-40 *Nonlinear Static Procedure*. The improved procedure differs from ATC-40 procedures in one important sense. The demand diagram used is different: the constant-ductility demand diagram for inelastic systems in the improved procedure versus the elastic demand diagram in ATC-40 for equivalent linear systems.

INTRODUCTION

The *Nonlinear Static Procedure* in ATC-40 and FEMA-274 documents is based on the capacity spectrum method (Freeman et al., 1975) which is used to determine the seismic deformation of an SDF system derived from the pushover curve. This method is based on the belief that the earthquake-induced deformation of an inelastic SDF system can be estimated satisfactorily by an iterative method requiring analysis of a sequence of equivalent linear SDF systems, thus avoiding the dynamic analysis of the inelastic SDF system.

The principal objective of this investigation is to develop improved simplified analysis procedures, based on capacity and demand diagrams, to estimate the peak deformation of inelastic SDF systems. These improved procedures use the well-established inelastic response (or design) spectrum. The idea of using the inelastic design spectrum in this context was suggested by Bertero (1995), and introduced by Reinhorn (1997) and Fajfar (1999).

EVALUATION OF NONLINEAR STATIC PROCEDURE

The excitation is characterized by the elastic design spectrum of Fig. 1 which is the median-plus-one-standard-deviation spectrum constructed by the procedures of Newmark and Hall (1982), as described in Chopra (1995; Section 6.9). The yield strength of each bilinear hysteretic system analyzed was chosen corresponding to an allowable ductility μ:

$$f_y = (A_y/g)w \tag{1}$$

where w is the weight of the system and A_y is the pseudo-acceleration corresponding to the allowable ductility and the vibration properties – natural period T_n and damping ratio ζ – of the system in its linear range of vibration. Given the properties T_n, ζ, and f_y and the elastic design spectrum, the earthquake induced

[1] *Dept. of Civil & Environmental Engieering, University of California, Berkeley, CA 94720, U.S.A.*
[2] *Dept. of Civil & Environmental Engieering, Cal Poly State University, San Luis Obispo, CA 93407, U.S.A.*

deformation of the system can be determined as described in Chopra (1995: Section 7.6). Utilized in such a procedure is a T_n -dependent relation between yield strength reduction factor R_y and μ.

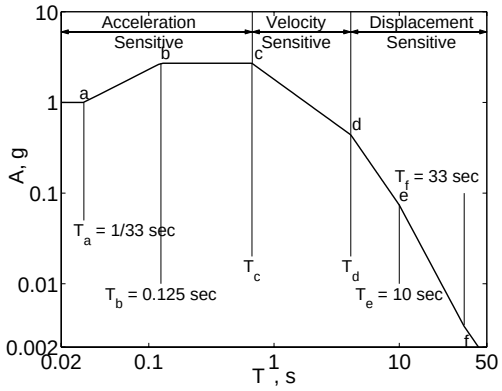

Figure 1. Newmark-Hall elastic design spectrum.

Presented in Fig. 2 are the deformations determined by using three different $R_y - \mu - T_n$ equations: Newmark and Hall (1982); Krawinkler and Nassar (1992) for elastoplastic systems; and Vidic, Fajfar and Fischinger (1994) for bilinear systems. The equations describing these relationships are presented in Chopra and Goel (1999). Observe that the three recommendations lead to similar results except for $T_n < 0.3$ sec , indicating that the inelastic design spectrum is a reliable approach to estimate the earthquake-induced deformation of yielding systems, reliable in the sense that different researchers have produced similar results.

The deformation estimates by the ATC-40 method, as determined by Chopra and Goel (1999), are also included in Fig. 2. Relative to the deformation value from inelastic design spectra, the percentage discrepancy in the approximate result is plotted in Fig. 3. The approximate procedure underestimates the deformation significantly, except for very long periods ($T_n > T_f$ in Fig. 1).

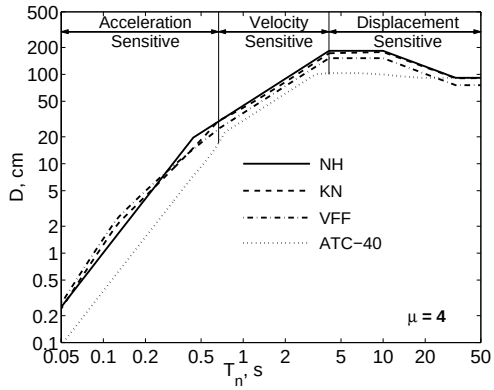

Figure 2. Deformation of inelastic systems (μ= 4) determined from inelastic design spectra using ATC-40 Procedure and three $R_y - \mu - T_n$ equations: Newmark-Hall (NH), Krawinkler-Nassar (KN), and Vidic-Fajfar-Fischinger (VFF).

In passing, note that the ATC-40 procedure is deficient relative to even the *elastic* design spectrum in the velocity-sensitive and displacement-sensitive regions $(T_n > T_c)$. For T_n in these regions, the peak deformation of an inelastic system can be estimated from the elastic design spectrum, using the well-known equal-displacement rule (Veletsos and Newmark, 1960). However, the ATC-40 procedure requires analyses of several equivalent linear systems and still produces worse results.

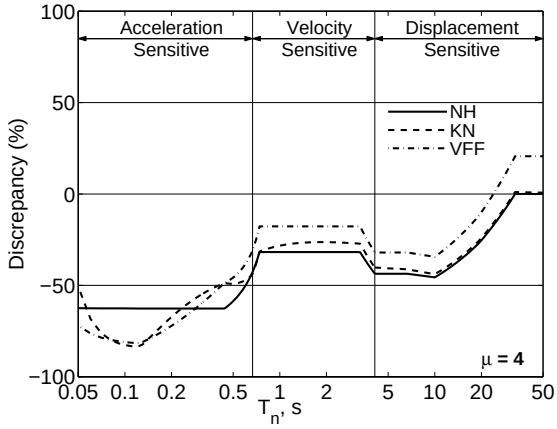

Figure 3. Discrepancy in deformations computed by ATC-40 procedure relative to three different (NH, KN, VFF) inelastic design spectra; μ = 4.

IMPROVED PROCEDURES

Inelastic Design Spectrum

A constant-ductility spectrum for a bilinear hysteretic system is a plot of A_y versus T_n for selected values of μ. The pseudo-acceleration A_y is related to the yield strength f_y, by Eq. (1). The yield strength reduction factor is given by

$$R_y = \frac{f_o}{f_y} = \frac{A}{A_y} \tag{2}$$

where

$$f_o = \left(\frac{A}{g}\right) w \tag{3}$$

is the minimum yield strength required for the structure to remain elastic during the earthquake; *A* is the pseudo-acceleration ordinate of the elastic design spectrum at (T_n, ζ).

A constant-ductility design spectrum is established by dividing the elastic design spectrum by appropriate ductility-dependent reduction factors that depend on T_n. The earliest recommendation for the reduction factor, R_y (Eq. 2), goes back to the work of Veletsos and Newmark (1960), which is the basis for the inelastic design spectra developed by Newmark and Hall (1982). Starting with the elastic design spectrum of Fig. 1 and these $R_y - \mu$ relations for acceleration-, velocity-, and displacement-sensitive spectral regions, the inelastic design spectrum constructed by the procedure described in Chopra (1995, Section 7.10), is shown in Fig. 4a.

In recent years, several recommendations for the reduction factor have been developed (e.g., Krawinkler and Nassar, 1992; Vidic, Fajfar, and Fischinger, 1994). Based on two of these recommendations, the inelastic design spectra are also shown in Fig. 4a.

Inelastic Demand Diagram

The inelastic design spectra of Fig. 4a will be plotted in the *A*-*D* format to obtain the corresponding demand diagrams. The peak deformation *D* of the inelastic system is given by:

$$D = \mu \frac{1}{R_y} \left(\frac{T_n}{2\pi} \right)^2 A \tag{4}$$

Using Eq. (4), D is determined corresponding to the three inelastic design spectra in Fig. 4a. Such data pairs (A_y ,D) are plotted to obtain the demand diagram for inelastic systems (Fig. 4b).

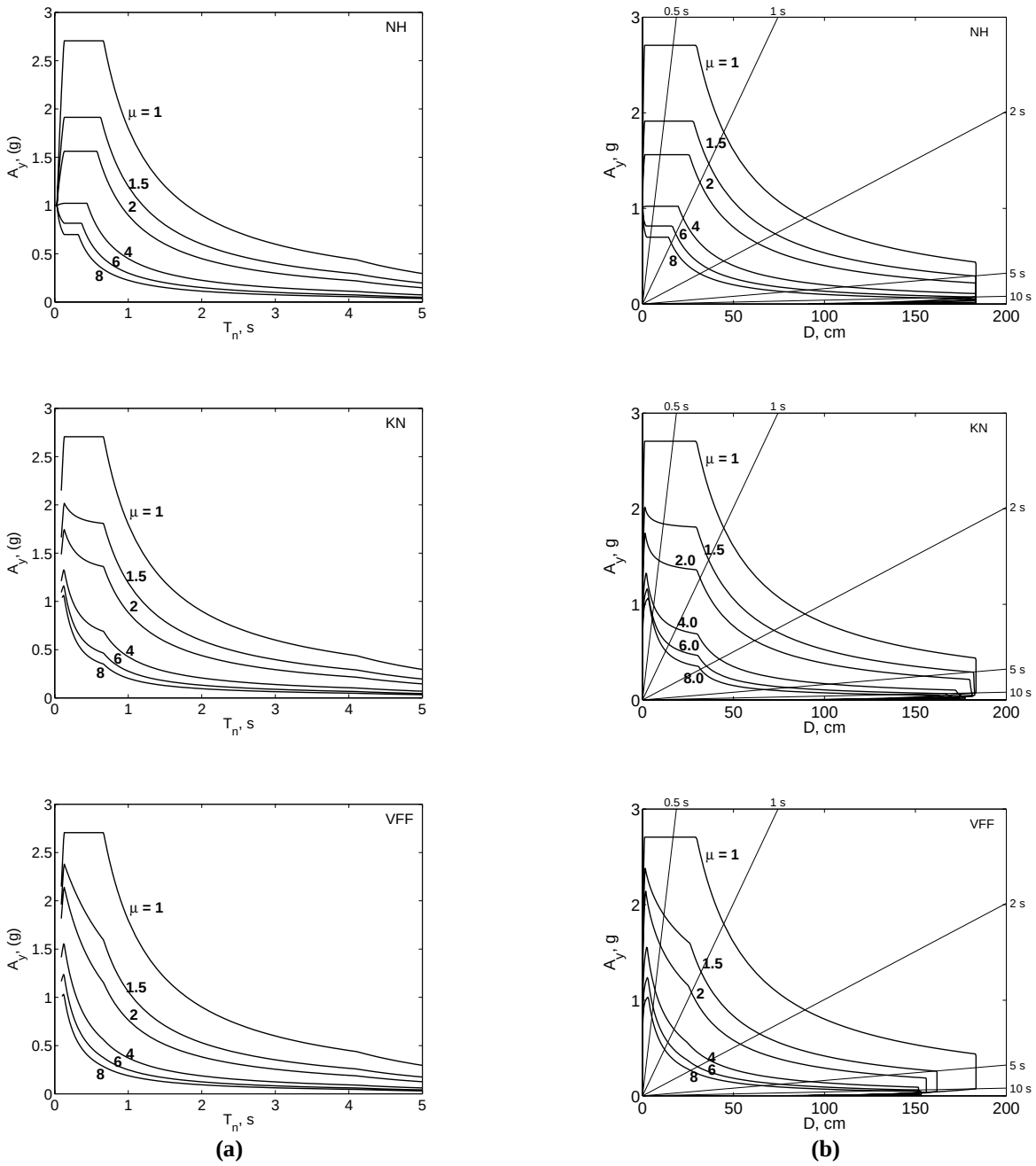

Figure 4. (a) Inelastic design spectra and (b) Inelastic demand diagrams, based on three different (NH, KN, VFF) recommendations.

Improved Procedure

This procedure, which uses the demand diagram for inelastic systems (Fig. 4b), will be illustrated with reference to six elastoplastic systems defined by two values of T_n = 0.5 and 1.0 sec and three different yield strengths, given by Eq. (1) corresponding to μ = 2, 4, and 6, respectively. For systems with T_n = 0.5 sec, $f_y \div w =$ 1.5624, 0.8992, and 0.5995 for μ = 2, 4, and 6, respectively. The corresponding values for systems with T_n = 1

sec are $f_y \div w =$ 0.8992, 0.4496, and 0.2997. Superimposed on the demand diagrams are the capacity diagrams for three inelastic systems with T_n = 0.5 sec (Fig. 5a) and T_n = 1.0 sec (Fig. 5b). The yielding branch of the capacity diagram intersects the demand diagram for several μ values. One of these intersection points, which remains to be determined, will provide the deformation demand. At the one relevant intersection point, the ductility factor calculated from the capacity diagram should match the ductility value associated with the intersecting demand curve. Determined according to this criterion, the deformation for each system is noted in Fig. 5. This result will be essentially identical to that given by Eq. (4). Implementation of this procedure is illustrated for two systems.

Examples

The yield deformation of System 1 is $u_y = 3.724\,\text{cm}$. The yielding branch of the capacity diagram intersects the demand curves for μ = 1, 2, 4, 6, and 8 at 133.93 cm, 66.96 cm, 33.48 cm, 22.3 cm, and 16.5 cm, respectively (Fig. 5a). Dividing by u_y, the corresponding ductility factors are: 133.93÷3.724=35.96 (which exceeds μ = 1 for this demand curve), 66.96÷3.724=17.98 (which exceeds μ = 2 for this demand curve), 33.48÷3.724=8.99 (which exceeds μ = 4 for this demand curve), 22.3÷3.724=6 (which matches μ = 6 for this demand curve), and 16.5÷3.724=4.43 (which is smaller than μ = 8 for this demand curve). Thus, the ductility demand is 6 and the deformation of System 1 is *D* = 22.3 cm.

For System 3, $u_y = 9.681\,\text{cm}$. The yielding branch of the capacity diagram intersects the demand curve for μ = 1 at 51.34 cm (Fig. 5a). The corresponding ductility factor is 51.34÷9.681=5.3, which is larger than the μ = 1 for this demand curve. The yielding branch of the capacity diagram also intersects the demand curve for μ = 2 continuously from 9.681 cm to 25.2 cm, which correspond to ductility factors of 1 to 2.6. The intersection point at 19.29 cm corresponds to ductility factor = 19.39÷9.681=2 which matches μ = 2 for this demand curve. Thus, the ductility demand is 2 and the deformation of System 3 is *D* = 19.39 cm.

Observe that for the presented examples, the ductility factor at the intersection point matched exactly the ductility value associated with one of the demand curves because the f_y values were chosen consistent with the same μ values for which the demand curves have been plotted. In general this is not the case and interpolation between demand curves for two μ values would be necessary. Alternatively, the demand curves may be plotted at a finer μ interval avoiding the need for interpolation.

Comparison with ATC-40 Procedure A

The improved procedure just presented gives the deformation value consistent with the selected inelastic design spectrum, while retaining the attraction of graphical implementation of the ATC-40 Procedure A. The two procedures are similar in the sense that the desired deformation is determined at the intersection of the capacity diagram and the demand diagram. However, the two procedures differ fundamentally in an important sense; the demand diagram used is different: the constant-ductility demand diagram for inelastic systems in the improved procedure (Fig. 5) versus the elastic demand diagram in ATC-40 Procedure A for equivalent linear systems.

IMPROVED PROCEDURE: NUMERICAL VERSION

The improved procedure presented in the preceding section was implemented graphically, in part, to highlight the similarities and differences relative to the *Nonlinear Static Procedure* in the ATC-40 report. However, this graphical feature is not essential and the procedure can be implemented numerically. Such a procedure using $R_y - \mu - T_n$ equations is outlined in this section. While space limitation does not permit presentation of these equations (Chopra and Goel, 1999), they are plotted in Figures 6a and 6b. Plots of R_y versus T_n for selected values of μ are shown in Fig. 6a and of μ versus T_n for selected values of R_y in Fig. 6b. Observe the similarity among the three sets of results, indicating consensus among different researchers.

The peak deformation of systems 1 to 6 (Table 1) are determined using $R_y - \mu - T_n$ relations. Detailed calculations are presented in Chopra and Goel (1999: Appendix B) and the results are summarized in Table 1.

Observe that the deformation values computed using $R_y - \mu - T_n$ equations are identical to those determined by the graphical procedure (Fig. 5) except for round-off differences.

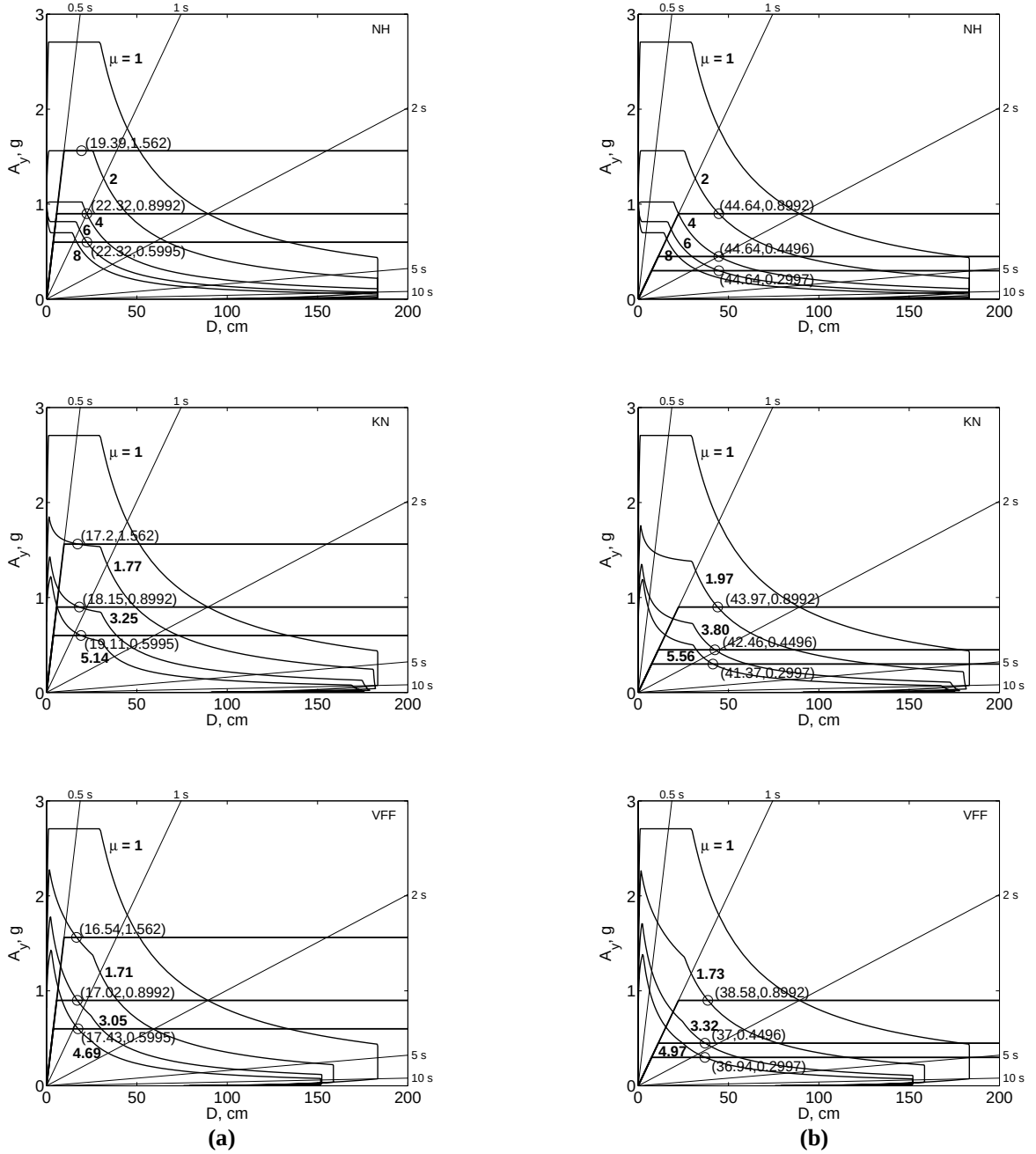

Figure 5. Application of Improved Procedure using three different (NH, KN, VFF) inelastic design spectra: (a) Systems 1 to 3, and (b) Systems 4 to 6.

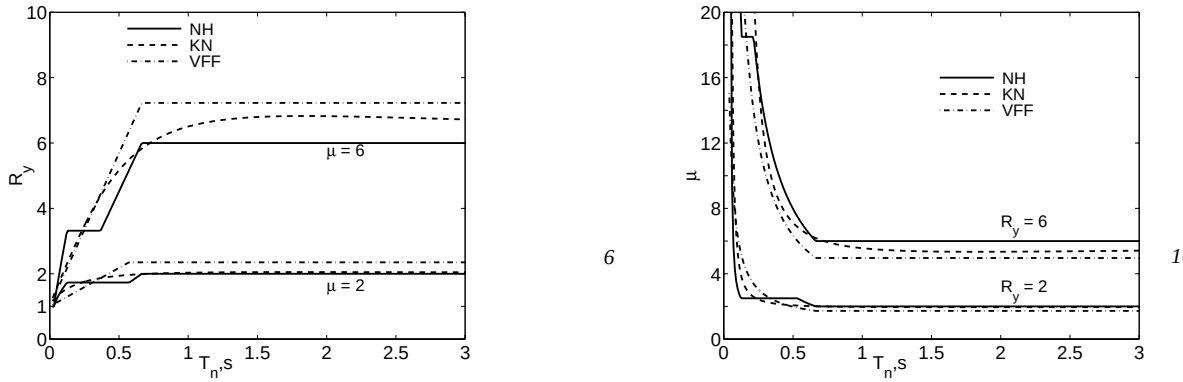

Figure 6. (a) Variation of R_y with T_n for selected ductility values , and (b) variation of μ with T_n for selected R_y values based on three different (NH, KN, VFF) recommendations.

Table 1. Results from numerical implementation of improved procedure using three $R_y - \mu - T_n$ equations.

System Properties						Newmark-Hall		Krawinkler-Nassar		Vidic et al.	
System	T_n (s)	A (g)	A_y (g)	u_y (cm)	R_y	μ	D	μ	D	μ	D
1	0.5	2.7062	0.5995	3.7202	4.51	5.99	22.29	5.14	19.11	4.69	17.43
2			0.8992	5.5803	3.01	3.99	22.29	3.25	18.15	3.05	17.02
3			1.5624	9.6962	1.73	2.00	19.39	1.77	17.20	1.71	16.54
4	1	1.7984	0.2997	7.4403	6.00	6.00	44.64	5.56	41.37	4.97	36.94
5			0.4496	11.160	4.00	4.00	44.64	3.80	42.46	3.32	37.00
6			0.8992	22.321	2.00	2.00	44.64	1.97	43.97	1.73	38.58

CONCLUSIONS

This investigation of capacity-demand-diagram methods to estimate the earthquake-induced deformation of inelastic SDF systems has led to the following conclusions:

1. The ATC-40 procedure significantly underestimates the deformation of inelastic systems for a wide range of T_n and μ values compared to the value determined from the inelastic design spectrum using three different $R_y - \mu - T_n$ equations, all of which provided similar results.
2. An improved capacity-demand-diagram method that uses the well-known constant-ductility design spectrum for the demand diagram has been developed and illustrated by examples. When both capacity and demand diagrams are plotted in the *A-D* format, the yielding branch of the capacity diagram intersects the demand curves for several μ values. The deformation is given by the one intersection point where the ductility factor calculated from the capacity diagram matches the value associated with the intersecting demand curve.
3. The improved method can be conveniently implemented numerically if its graphical features are not important to the user. Such a procedure, based on equations relating R_y and μ for different T_n ranges, has been presented and illustrated by examples using three different $R_y - \mu - T_n$ relations.

ACKNOWLEDGEMENT

This research investigation is funded by the National Science Foundation under Grant CMS-9812531, a part of the U.S.-Japan Cooperative Research in Urban Earthquake Disaster Mitigation. This financial support is gratefully acknowledged.

REFERENCES

Applied Technology Council (1996). *Seismic Evaluation and Retrofit of Concrete Buildings*. Report ATC 40, November.

Bertero, V. V. (1995). "Tri-service manual methods" in *Vision 2000*, Part 2, Appendix J. Structural Engineers Association of California, Sacramento.

Chopra, A. K. (1995). *Dynamics of Structures: Theory and Applications to Earthquake Engineering*, Chapters 6, 7, and 13, Prentice Hall, New Jersey.

Chopra, A. K. and Goel, R. K. (1999). *Capacity-Demand-Diagram Methods for Estimating Seismic Deformation of Inelastic Structures: SDF Systems*. Report No. PEER-1999/02, Pacific Earthquake Engineering Research Center, University of California, Berkeley, April.

Fajfar, P. (1999). “Capacity Spectrum Method based on Inelastic Spectra.” Earthquake Engineering and structural Dynamics, to appear.

FEMA (1997). *NEHRP Guidelines for the Seismic Rehabilitation of Buildings*, FEMA 273; and *NEHRP Commentary on the Guidelines for the Seismic Rehabilitation of Buildings*, FEMA 274, October, Federal Emergency Management Agency, Washington, D.C.

Freeman, S. A., Nicoletti, J. P., and Tyrell, J. V. (1975). “Evaluations of existing buildings for seismic risk - A case study of Puget Sound Naval Shipyard, Bremerton, Washington.” *Proceedings of 1st U.S. National Conference on Earthquake Engineering*, EERI, Berkeley, 113-122.

Krawinkler, H., and Nassar, A. A. (1992). “Seismic design based on ductility and cumulative damage demands and capacities.” in *Nonlinear Seismic Analysis and Design of Reinforced Concrete Buildings*, P. Fajfar and H. Krawinkler, Eds., Elsevier Applied Science, New York, 1992.

Newmark, N. M., and Hall, W. J. (1982). *Earthquake Spectra and Design*. Earthquake Engineering Research Institute, Berkeley, CA.

Reinhorn, A. M. (1997). “Inelastic analysis techniques in seismic evaluations.” P. Fajfar and H. Krawinkler (eds.), *Seismic design methodologies for the next generation of codes*, Balkema, Rotterdam, 277-287.

Veletsos, A. S., and Newmark, N. M. (1960). “Effects of inelastic behavior on the response of simple system to earthquake motions.” *Proceedings of the 2nd World Conference on Earthquake Engineering*, Japan, Vol. 2, pp. 895-912.

Vidic, T., Fajfar, P., and Fischinger, M. (1994). “Consistent inelastic design spectra: strength and displacement.” *Earthquake Engineering and Structural Dynamics*, Vol. 23, No. 5, pp. 507-521.